Physicochem. Probl. Miner. Process. 53(1), 2017, 173−183

www.minproc.pwr.wroc.pl/journal/

Physicochemical Problems of Mineral Processing

ISSN 1643-1049 (print)
ISSN 2084-4735 (online)

Received March 3, 2016; reviewed; accepted June 20, 2016

INSIGHTS INTO HYDRODYNAMICS OF SPINNING FLUIDS REACTOR

Adam DARGACZ, Robert ARANOWSKI

Gdansk University of Technology, Chemical Faculty, Department of Chemical Technology, Narutowicza 11/12, 80-233 Gdansk, Poland

Abstract: Spinning fluids reactor (SFR) is one of the most efficient gas-liquid contacting system with high potential of application in many fields. The unique solution of SFR is the contacting of two spinning fluids which generated centrifugal force. The aim of this study was to investigate the pressure field distribution on the inner surface of reactors dispersing element. Obtained results confirm the high heterogeneity of the field pressure in the reactor system with a cylindrical wall. This is due to the low tangential force generated by rotating liquid on a cylindrical wall, and pressure drop in the locations of surface irregularities. The change of the sparger element to conical shape element increases the pressure exerted by fluid on the wall. In this case the effects of solid particles and inequality in the fluid flow are negligibly small compared to the measured pressure exerted on the sparger element.

Keywords:

Introduction

In mineral processing and chemical technology mass transfer and separation operations take place most frequently in multiphase systems (Ahmed and Jameson, 1985; Bokotko et al., 1996; Rao, 2013; Rubio et al., 2002), particularly at the gas-liquid interphase (Anderson, 1959; Bokotko et al., 1996; Bokotko et al., 1997; Bokotko et al., 1998). Due to very voluminous streams the compactness of the reactor is here of substantial importance (Bokotko et al., 2005). The spinning fluids reactor (SFR) represents a design which fulfils such expectations (Miller et al., 2012). The unique solution of the technology is contacting of two spinning fluids aimed at rapid mass transfer accompanied by a single or multiple chemical reactions taking place in either one or the two spinning streams (Hupka et al., 1999). The technology, which has been tested using mobile systems for recovery of cyanides from aqueous solutions from gold mining (field tests in the USA) and toluene recovery from air during

http://dx.doi.org/10.5277/ppmp170114

chemical synthesis (field tests in Poland), occurred to be superior to competing technologies (Hupka et al., 2005).

Principle of reactor operation

In the spinning fluids reactor (SFR) system two major changes were made. The first one concerns sparger element and the second is connected with the flow path of the gaseous phase. In the ash-sparged hydrocyclone (ASH) plastic or metal porous tube was used as the sparger with pore size from 60 to several-hundred microns (Bokotko et al., 1997; Miller, 1981; Miller and Das, 1996; Miller and Yi, 1989). When the air flowed through the porous wall a high pressure drop occured (Bokotko, 2000; Bokotko and Hupka, 1996). In the SFR system, instead of plastic tube, a metal mesh was used. It changed drastically the resistance of air flow but also caused new problem – a heterogeneity of the pressure drop along the Z axis of the sparger element. This effect results in tangential force generated by the liquid phase flow on inner wall of the sparger. In this regards one of the most important parameter for properly working SFR is the pressure field distribution on the inner surface of the reactor sparger element.

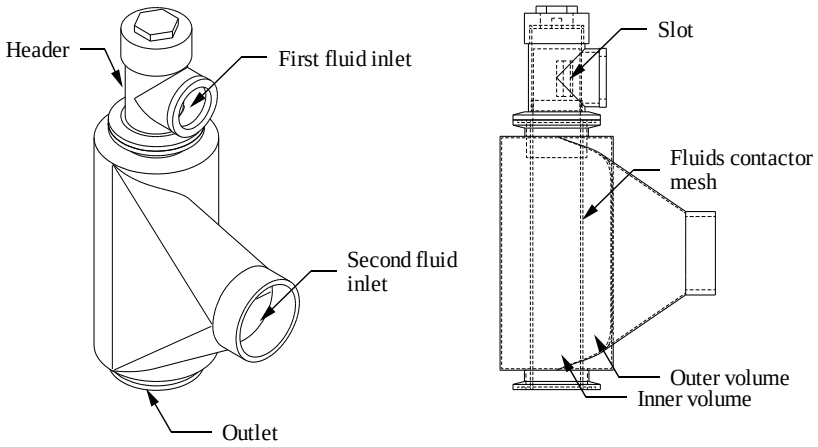

Fig. 1. Partial see-through view of a variant of SFR

The flow of liquid in the SFR is very complex and radically different from that in conventional hydrocyclones. Thus, investigations of flow characteristics are not easy because of the reactor construction. Earlier studies showed that the thickness of the liquid did not depend on the flow rate and was approximately 10% of the internal radius of the reactor. These results were compared with the values obtained by using Taylor's theory (Miller and Kinneberg, 1984). The calculated values were very similar to those obtained experimentally (Leliński et al., 1996). This theory, however, does not allow for determination of changes in velocity along the vertical axis of the reactor.

According to Miller et al. (1985) in the cross section of the cylindrical part, the distribution of the liquid velocity and liquid layer thickness is the same, regardless of the liquid flow rate (Hupka et al., 1996). Applying the rule of conservation of momentum, linear velocity changes can be calculated along the axis of reactor as an effect of friction forces. Liquid flows down the inner walls of the reactor swirling. Speed of this movement u can be divided into two components: the tangential u_t and vertical u_o velocities:

$$\vec{u} = \vec{u}_t + \vec{u}_o.$$

The tangential velocity is the dominant velocity component and it also determines the centrifugal force applied to the liquid stream. Pressure of liquid acted on the walls determines the friction forces which act on both the vertical and tangential velocity, causing its decrease in a similar rate. As a result, the fluid velocity direction remains practically the same throughout the whole length of the reactor.

The velocity profile has a significant impact on the centrifugal force exerting pressure on the reactors walls, which in consequence affects the size of formed gas bubbles, pressure inside them and model of their release from the surface. The pressure distribution in a reactor varies with different designs. The highest pressure is located at the wall. The pressure decreases with the reduction of the rotational radius because of the increasing tangential velocity. The pressure drop over the reactor is caused by the area changes, wall friction, change of flow direction and dissipation in the outlet.

Taking a very small volume of the spinning liquid with vertical area dA and thickness dr, the centrifugal force would be formulated as:

$$\mathrm{d}F = \rho \mathrm{d}A \mathrm{d}r \frac{u_t^2(r)}{r}. \tag{1}$$

From the equilibrium law, we assume that dF/dA should be equal to dp_r, so:

$$\frac{\mathrm{d}p_r}{\mathrm{d}r} = \rho \frac{u_t^2(r)}{r} = \rho \omega^2 r \tag{2}$$

where ω is the angular velocity of rotating liquid. The above equation indicates that the radial pressure gradient depends on the centrifugal acceleration.

Experimental

The aim of this study was to investigate the pressure field distribution on the inner surface of the reactors dispersing element. Three shapes of the dispersing element were used during experiments: cylindrical and two truncated cones with lateral height inclined at 88.5 and 87 degrees from the base of the cone. The pressure measurements were made with piezoelectric sensor MPX5100DP from Motorola. These sensors are characterized by a high accuracy and linearity in the range from 0 to 100 kPa. The study was set on model imitating a cyclone reactor dispersive element. Head with

inner diameter 50.8 mm, 90 mm height and the dimensions of the inlet 20×7.5 mm have been mounted. Immobilised head was a base for attaching the models. One model made of a transparent tube with a diameter of 50 mm (2") and two cones made of a metal sheet. The cone height was determined by 35 mm diameter of the outlet to prevent the accumulation of fluid at the outlet and the appearance of liquid flow resistance. The entire length of the model has been equipped with copper tubes with an internal diameter of 4 mm and length of 15 mm mounted in line. For the first 18 cm the tubes were spaced 1 cm, and then every 2 cm down to the exit of the model. Sensors were attached to the model using polymer tubes with an internal diameter of 5 mm. Each pressure sensor has been equipped with a capacitor noise filter according to the manufacturer recommendations. In addition, all shielding of the signal cables were grounded. The sensors were supplied with a constant voltage of 5 V from stabilized power supply with accuracy less than 0.1 mV. The results were collected using a National Instruments card NI 6515. The results were saved in text files from 7 sensors simultaneously with a dedicated self-executable program.

The program contained a calibration equation developed individually for each sensor and saved into the file voltage values converted to pressure values. Four programs were created to store data for a total of 28 sensors collected in seven groups. Sensor calibration was performed on a system of hydrostatic pressure gauge U-tube and the high pressure air support. For pressures up to 6 kPa U-tube was filled with water, and for pressures from 6 kPa to 60 kPa mercury was used. Calibration results were collected in the same way as measurements and linear equations were determined of differential pressure signal from the output voltage signal.

Water was supplied to the research model by a Jacobsen's Tapflo pump. The study was conducted for five values of volumetric flow intensities respectively for 20, 30, 40, 50 and 60 dm^3/min. The flow control was followed by an electronic control unit coupled with a computer. The system controlled the frequency of the pump power supply according to the readings of the magnetic flow meter located at the pump outlet.

The first step was to approach the reference value of liquid flow and passing 1 minute for establishment of the flow conditions in the reactor. In the second step collecting results started for seven sensors simultaneously for about 30 seconds. Then, the attitude of the flow was changed and the procedure repeated. When results for all of the flows were collected, the program was changed to write data for the next group of seven sensors with the corresponding calibration equations and then measurements were repeated for all flows. When the results of all sensors were collected, the head of the model was rotated by 30 deg. This allowed for the measurement of pressure on the whole interior surface at 16 elevations and at 12 different rotations.

Pooled results for a single set location and flow were averaged and placed in a summary table. It contains the results for a single flow in accordance with the height and angle of the measuring point. The prepared map of results shows a reactor pressure fields of the cyclone with a sparger element shapes and the predetermined flow of liquid.

Results

The chart shown in Fig. 2 is a map of the pressure exerted on the sparger element model generated by a liquid flow of 20 dm^3/min. The colours correspond to the measured pressure values. As can be seen the pressure decreases along the vertical axis of the reactor with a decrease of the linear velocity of the liquid as a result of friction forces. At the first line of pressure sensors at height of 91 mm of the obtained results, in spite of theoretical considerations, there are not the highest pressures. These results can be explained by inaccuracy of head and sparger element diameter, what can create an error. Such inequality is present in any equipment with a segment-like construction and the presence of lower pressure zone has got to be expected in this area. Following the downward, a region of high pressure, between 0.4 and 0.8 kPa, occurs. From this level a systematic drop in the pressure occurs up to 0.1 kPa at the outlet of the liquid.

The cylindrical model is particularly vulnerable to phenomenon of detachment of the liquid from the surface of the walls. Present in the map the regions of negative pressure, caused by subatmospheric pressure which arise in the areas, generates a local vacuum reading. This is so because of a low linear velocity of liquid in comparison to the cone. In the case of the investigated model, inequalities came out by copper tubing assembly on the body tube. In a real application, this inequality can be the roughness of the sintered porous material, wire mesh element or solid particles from the circulating media attached to the surface. These places can be a source of gas bubbles with the largest diameter, and thus, adversely affecting the uniformity of the conditions of mass transfer across the reactor.

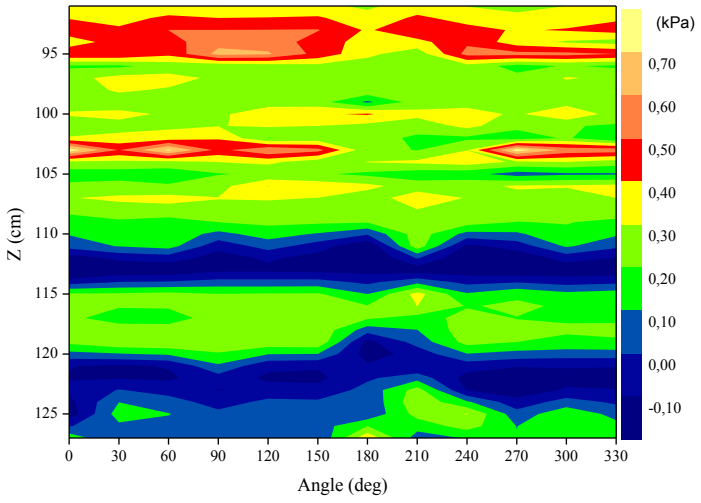

Fig. 2. Pressure distribution in cylindrical model at 20 dm^3/min liquid flow

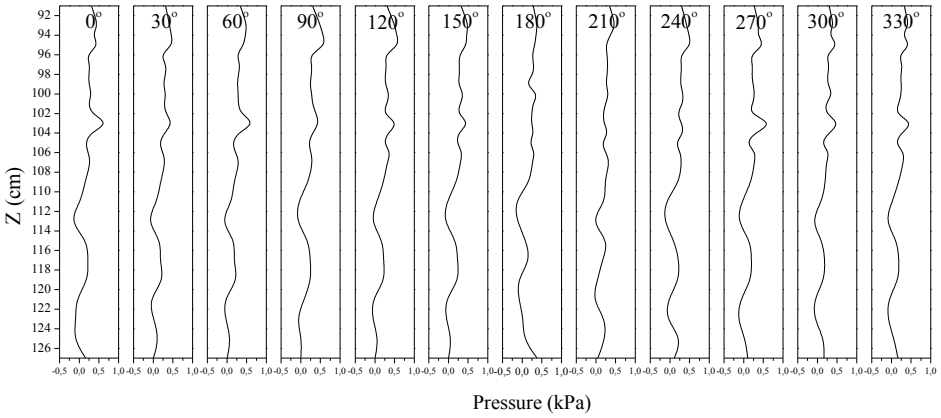

Fig. 3. Cross section of pressure field exerted on the sparger element

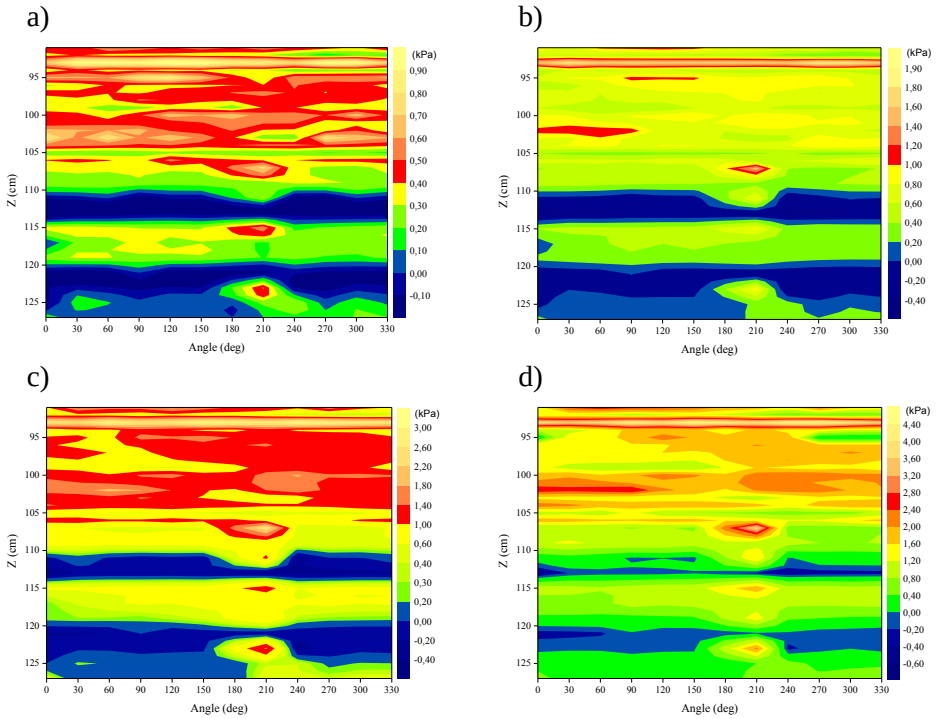

Fig. 4. Pressure distribution in cylindrical model at a) 30 dm^3/min, b) 40 dm^3/min, c) 50 dm^3/min, and d) 60 dm^3/min

The plots (Fig. 4) are showing pressure distribution for a cylindrical element at flows of 30, 40, 50 and 60 dm^3/min. With the increase of the flow, the pressure grows and for 60 dm^3/min it exceed 4 kPa. In the graph, it begins to be an apparent path of the liquid vortex. It is manifested by areas of slightly higher pressures starting at the

top left of the chart and extending to the level of 103 cm. In the following chart, this effect disappears as a result of too little pressure and a large number of disturbances. Starting from the level of 117 cm, the increase in the liquid flow has little effect on the increase in pressure and is identical, regardless of the flow.

The next graphs show the results of measurements of pressure in a model of the cone-shaped dispersing element with a truncated tip. The angle between radius and wall is 88.5 deg. Very clearly visible is the increase of pressure in the entire volume of the reactor. The maximum pressure is 0.8 kPa for 20 dm^3/min (Fig. 5) and is covering the better part of model area. In the same way the minimum pressure grows and one can see only one underpressure zone in the outlet.

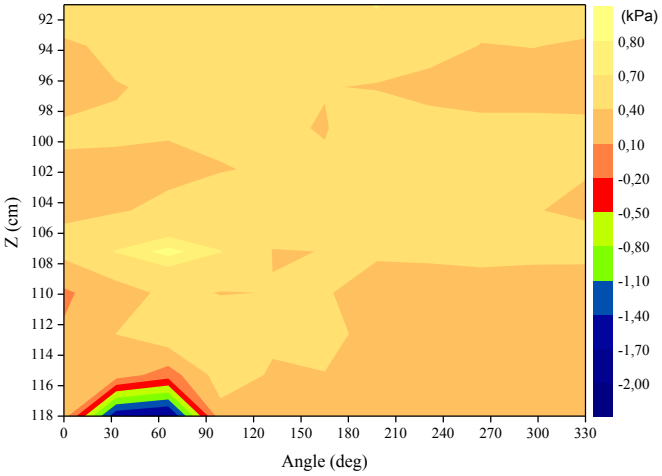

Fig. 5. Pressure distribution in 88.5 deg conical model at 20 dm^3/min liquid flow

It can be seen that the pressure at the top of reactor at 60 dm^3/min exceed 20 kPa (Fig. 6). Thus it is 5-fold higher at the same flow than in the cylindrical model. Another, very visible part, is the path of a rotating liquid. With the increase of flow, it becomes more visible and more regular. The pressure difference along the model also increase which increase visibility of the path of motion. These studies also confirm the conclusions of earlier studies about the flow of liquids in the cyclone flotation cell. The spin motion and associated with it the ratio of tangential and vertical velocities causes stability of the liquid layer thickness (Miller et al., 1985). In all graphs the same path of the fluid motion is visible.

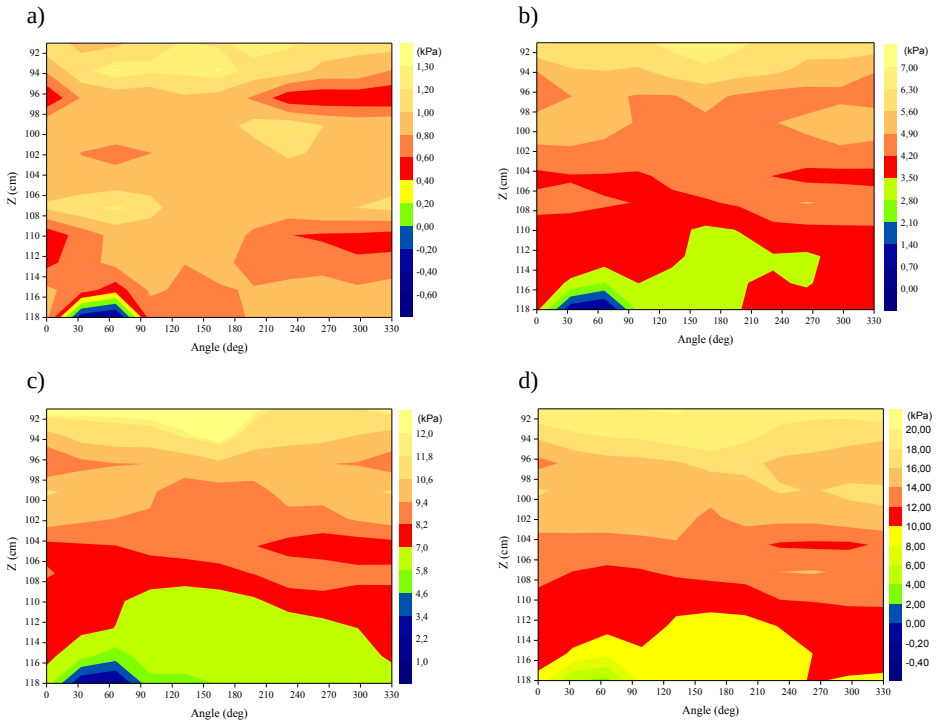

Fig. 6. Pressure distribution in 88.5 deg conical model at a) 30 dm^3/min, b) 40 dm^3/min, c) 50 dm^3/min, and d) 60 dm^3/min

The graphs also show the decreases in the amount of disruption of the flow which can be seen as the continuous-pressure between the points of measurements. This is mainly due to a low value of the interference pressure differences to the pressure exerted on the wall by the liquid. In contrast to the cylindrical shape, there is almost no vacuum readings. It is the result of a large centrifugal force of the spinning liquid and impact of additional pressure gradient due to the weight of the liquid inside the reactor acting on the walls. It should be noted that the lowest pressure at a flow of 60 dm^3/min is higher than the maximum pressure for the same liquid flow intensity in a cylindrical model.

Further results are collected on the model with the conical shape with angled wall 87° to the radius. Due to the limitation of the outlet, the diameter model is shorter than the other two. The following is a sequence of measurement results for the 20 dm^3/min (Fig. 6), 30, 40, 50 and 60 dm^3/min (Fig. 8) flows. As expected, the reduction in the angle of the cone resulted in a further increase in pressure. The maximum pressure ranged from 1.3 kPa to 29 kPa. Also motion track of liquid is very well visible in the graphs of the second cone model. In addition, a deepening in the pressure difference between the main and secondary liquid path occurs. Also there is a shorter stroke of

rotary motion from the previous cone due to a greater participation of velocity tangent to the axis in the linear velocity of the fluid.

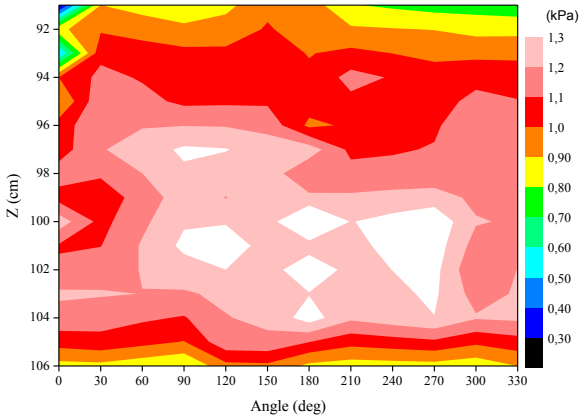

Fig. 7. Pressure distribution in 87 deg conical model at 20 dm^3/min liquid flow

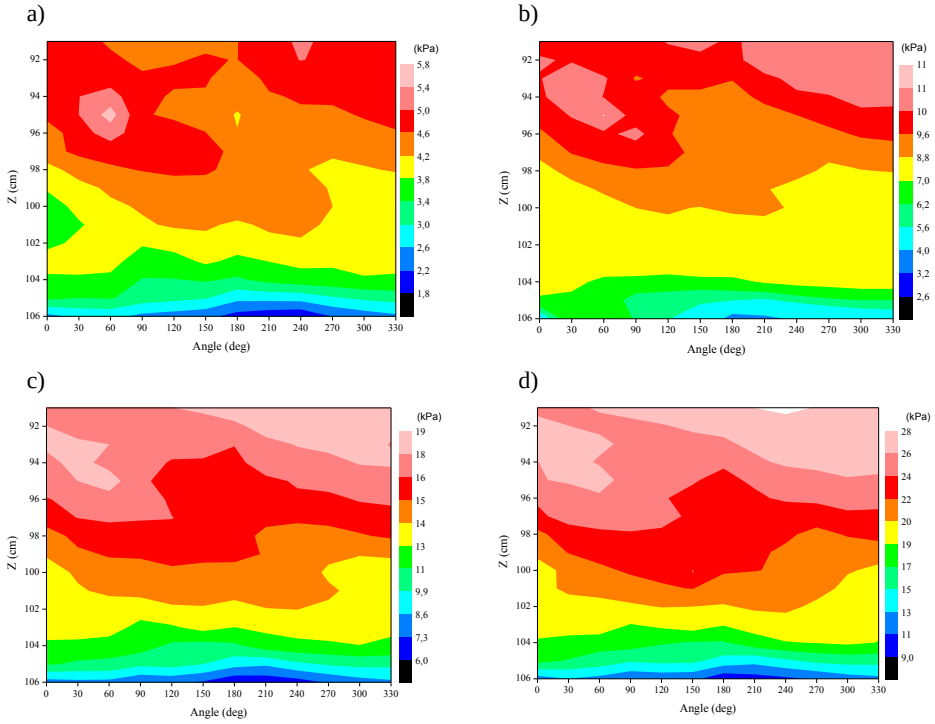

Fig. 8. Pressure distribution in 87 deg conical model at a) 30 dm^3/min, b) 40 dm^3/min, c) 50 dm^3/min, and d) 60 dm^3/min

It is worth noting an anomalous rotational motion at flow of 20 dm^3/min. The liquid does not perform the classical helical motion but accumulates in the middle of

the cone. Thus, the highest pressure reading in the middle of a research model and not in the upper part as in the other cases.

In the case of a conical shape in both cases we find areas of increased pressure drop just prior to departure from the reactor. It is caused by the proximity of the outlet and dissipation of the energy. The result is a gradual decline in the rotating fluid layer thickness due to the lack of flow resistance in the direction of the cone axis.

Conclusions

The obtained results confirm a high heterogeneity of the field pressure in the reactor system with a cylindrical wall. This is due to a low tangential force generated by the rotating liquid on a cylindrical wall and pressure drop in the locations of the surface irregularities. The change of the sparger element to a conical shape element increases the pressure exerted by the fluid on the wall. In this case the effects of solid particles and inequality in the fluid flow are negligibly small when compared to the measured pressure exerted on the sparger element.

The shape of the cone is not able to provide uniform pressure on the inner wall, over the entire length of the reactor. In the case of a conical shape of the sparger elements in both models, areas of increased pressure drop just prior to outlet of the SFR were found.

It was noted that the increase in the flow rate causes the presence of regions of higher pressure. This suggests the formation of overlay of liquid stream filaments. This is another element which introduces heterogeneity of pressure in the reactor. It can be probably eliminated by using the heads of several points of the liquid inlet spaced around the circumference which will be investigated in further studies.

The length of the sparger element of the SFR should be limited to 200 mm if the pressure drop field have to be in a narrow range of values because of a very rapid decrease in the tangential velocity. It should be also noted that the angle of the cone is limited, due to the outlet hole at the bottom of the reactor.

References

AHMED N., JAMESON G.J., 1985, *The effect of bubble size on the rate of flotation of fine particles*, Int J Miner Process 14(3), 195-215.

ANDERSON R.O., 1959, *A Modified Flotation Technique for Sorting Bottom Fauna Samples*, Limnol Oceanogr 4(2), 223-225.

BOKOTKO R., 2000, *Investigation of Mass Transfer Efficiency in Air Sparged Hydrocyclone and Bubbles Size Distribution Consideration*, doctoral dissertation, Gdansk University of Technology, Gdansk (in Polish).

BOKOTKO R., HUPKA J., 1996, *Efficiency of Water Aeration in Air Sparged Hydrocyclone*, Chem Eng Equip 35(2), 15-17 (in Polish).

BOKOTKO R., HUPKA J., LELINSKI D., MILLER J.D., 1996, *Separation of Oil-Containing Particles from Water in Cyclone Flotation Machine*, Envir Sci R 51, 155-164.

BOKOTKO R., HUPKA J., LELINSKI D., MILLER J.D., 1997, *Flotation of Fine Coke Particles from Fly Ash,* Physicochem Probl Mi 31, 221-228.

BOKOTKO R., HUPKA J., MARCHLIK A., 1998, *Sulphur Dioxide Separation in Air Sparged Hydrocyclone*, 2nd International Science Conference Theory and Practice in Environmental Protection, Szczyrk, Poland, 78-79 (in Polish).

BOKOTKO R.P., HUPKA J., MILLER J.D., 2005, *Flue gas treatment for SO2 removal with air-sparged hydrocyclone technology*, Environ. Sci. Technol. 39(4), 1184-1189.

HUPKA J., BOKOTKO R., LELINSKI D., MILLER J.D., 1996, *Bubble Size Distribution in Air-Sparged Hydrocyclone*, Recent Advances in Coal Processing, 801- 804, 811-812.

HUPKA J., DĄBROWSKI B., MILLER J.D., HALBE D., 2005, *Air-Sparged Hydrocyclone (ASH) Technology for Cyanide Recovery*, Miner. Metall. Process 22(3), 135-140.

HUPKA J., ZALESKA A., ARTUNA E., BOKOTKO R., TYSZKIEWICZ H., BIZIUK M., 1999, *Degradation of Almost Non-Soluble Organics in Gas-Sparged Reactor*, 2nd International Conference "Analysis and Utilization of Oily Wastes"AUZO'99, Jurata, Poland, 1-6.

LELINSKI D., BOKOTKO R., HUPKA J., MILLER J.D., 1996, *Bubble Generation in Swirl Flow During Air Sparged Hydrocyclone Flotation*, Minerals and Metallurgical Processing Journal 5, 87-92.

MILLER, J.D., 1981, *Air-Sparged Hydrocyclone and Method*, US patent 4,279,743.

MILLER J.D., DAS A.R., 1996, *Swirl Flow Characteristics and Froth Phase Features in Air-Sparged Hydrocyclone Flotation as Revealed by X-ray CT Analysis*, Int J Miner Process 47, 251-274.

MILLER J.D., HUPKA J., ARANOWSKI R., 2012, *Spinning Fluids Reactor*, International patent, PCTU509/52432.

MILLER J.D., KINNEBERG D.J., 1984, *Fast Flotation with an Air-Sparged Hydrocyclone*, MINTEK 50 International Conference on Recent Advences in Mineral Science and Technology, Johannesburg, South Africa, 373-383.

MILLER J.D., UPADRASHTA K.R., KINNEBERG D.J., GOPALAKRISHNAN S., 1985, *Fluid Flow Phenomena In the Air-Sparged Hydrocyclone*, XV International Mineral Processing Congress, Cannes, France, GEDIM, 87-99.

MILLER J.D., YI Y., 1989, *Air Sparged Hydrocyclone Flotation Apparatus and Methods for Separating Particles from a Particulate Suspension*, US patent, US 4838434 A.

RAO S.R., 2013, Surface Chemistry of Froth Flotation: Volume 1: Fundamentals, Springer US.

RUBIO J., SOUZA M.L., SMITH R.W., 2002, *Overview of flotation as a wastewater treatment technique*, Miner Eng 15(3), 139-155.